COVER SHEET

Paper Number: 137

Title: **VCCT with Progressive Nodal Release for Simulating Mixed-Mode Delamination: Formulation, Algorithmic Improvements and Implications**

Authors: G.E. Mabson
N.V. De Carvalho
R. Krueger

ABSTRACT

To simulate the propagation of cracks using the Virtual Crack Closure Technique (VCCT), intermediate crack positions between existing node pairs can be modeled by progressively releasing the nodes using fracture mechanics principles. This approach has been implemented in commercial software and can be applied to simulate delamination growth. Recent research has provided insight into the synchronized mixed mode nodal release, extending and formalizing the methodology for delamination growth. This paper documents the development of the Jacobians associated with delamination propagation under quasi-static mixed-mode conditions, leading to improvements in convergence of the implicit nonlinear solvers used.

INTRODUCTION

Within the Finite Element Method framework, Virtual Crack Closure Technique (VCCT) (e.g., [1-4]) and Cohesive Zone (CZ) approaches (e.g., [5, 6]) have become the most accepted techniques for simulating delamination propagation in composites, and have reached sufficient maturity to be available in several commercial simulation software packages. Modeling crack growth in an automated fashion, based on the energy release rates computed using VCCT, requires a separate strategy.

An approach [7] was proposed in which intermediate crack positions, which do not conform to the mesh, are accommodated by allowing the nodes to be released progressively. The approach was implemented via an interface element [7, 8] and applied to the simulation of delamination growth in 2D. A similar approach has been implemented in Abaqus/Standard [9] and can be applied to simulate delamination growth in 3D, but is presently limited to quasi-static applications. Recent progress on the NASA Advanced Composites Project (ACP), gives insight to the synchronized mixed

G.E. Mabson, Boeing Research and Technology, Seattle, WA, 98124
N.V. De Carvalho and R. Krueger, National Institute of Aerospace, 100 Exploration Way, Hampton, VA, 23666.

mode nodal release based on fracture mechanics principles [10], extending and formalizing the methodology proposed in [7] to enable modeling of mixed-mode fatigue delamination growth in 3D.

The amount of CPU time resulting from the required number of iterations for convergence is often problematic in many implicit progressive damage analysis procedures. Based on the formulation proposed in [7, 10] the present work focuses on obtaining analytical expressions for the Jacobian, to promote good convergence behavior and hence enable more difficult problems to be efficiently solved.

METHODOLOGY

The present section provides details of the VCCT methodology, including the procedures used to determine the energy release rates, the crack growth increment, and the progressive nodal release. In addition, details on the calculation of the Jacobians are provided. The methodology was implemented via the user element subroutines interface in ABAQUS.

Virtual Crack Closure Technique

For each node i at the crack front, (see Fig. 1), the energy release rates are calculated using the classic VCCT expressions:

$$\begin{aligned} G_I^{i,j} &= \frac{1}{2A^i} F_z^i \delta_z^j \\ G_{II}^{i,j} &= \frac{1}{2A^i} F_x^i \delta_x^j \\ G_{III}^{i,j} &= \frac{1}{2A^i} F_y^i \delta_y^j \end{aligned} \tag{1}$$

where F_k^i designates the forces obtained at node i along the directions $k = \{x, y, z\}$ and δ_k^j is the displacement jump computed at an adjacent node j:

$$\delta_k^j = u_k^{j^+} - u_k^{j^-} \tag{2}$$

where $u_k^{j^+}$ and $u_k^{j^-}$ are the displacement computed at the top and bottom surface of the interface at the nodal position j. The area A^i is defined by:

$$A^i = a_l^i a_w^i \tag{3}$$

where a_l^i and a_w^i are defined as illustrated in Fig. 1. The total energy release rate can be obtained by:

$$G_T^{i,j} = G_I^{i,j} + G_{II}^{i,j} + G_{III}^{i,j} \tag{4}$$

The energy release rate determination is automated by Eq. (4) for all adjacent node pairs j that have been completely released. Finally, the maximum energy release rate associated with node pair i is obtained by determining the maximum of the energy release rates computed using the displacement jump determined at each of the four immediately adjacent nodes, j to $j+3$:

$$G^i_{T_{max}} = max\{G^{i,j}_T, \dots, G^{i,j+3}_T\} \tag{5}$$

In the case illustrated in Fig. 1, only node j will have a nonzero displacement jump since nodes $j+1$, $j+2$ and $j+3$ are not in the crack wake, therefore $G^i_{T_{max}} = G^{i,j}_T$. Note however, that in a general case, the displacement jumps at nodes $j+1$, $j+2$ and $j+3$ may not be zero.

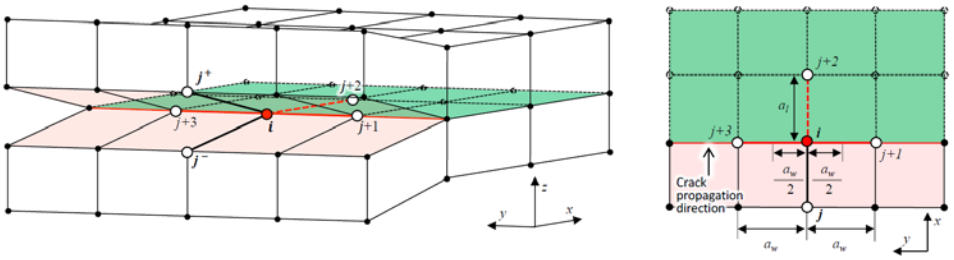

(a) 3D view (deformed) (b) Planar view (un-deformed)

Fig. 1 Crack front illustration and nomenclature.

Progressive Release

For a given material model, assume the crack grows past the node position i to some intermediate position. In order to represent that propagation, a kinematic constraint is inserted between the top and bottom surface nodes at the nodal position i, which can be thought of as springs connecting their degrees of freedom. The stiffness of these springs is decreased as required, progressively releasing the top and bottom surface nodes at the nodal position i. This procedure is illustrated in Fig. 2. Here, the progressive nodal release is intended to represent intermediate crack positions between node pairs, but is not a material constitutive response as in cohesive element formulations. This progressive release procedure results in a region across the crack front, where nodes may be at an intermediate stage of release, held by springs with different stiffnesses. While this region is akin to a process zone obtained in cohesive element formulations, the length of this process zone will not exceed the distance between node pairs. The need for the progressive release will be highlighted in the results section.

Consider a pure mode I loading, i.e., $G_{I_{max}} = G^i_{T_{max}}$. Assume that the energy release rate is such that the crack starts to grow, and designate that energy release rate $\widetilde{G_I}$ given by:

$$\widetilde{G_I} = \frac{F^i_{z_{max}} \delta^j_{z_{max}}}{2A^i} \tag{6}$$

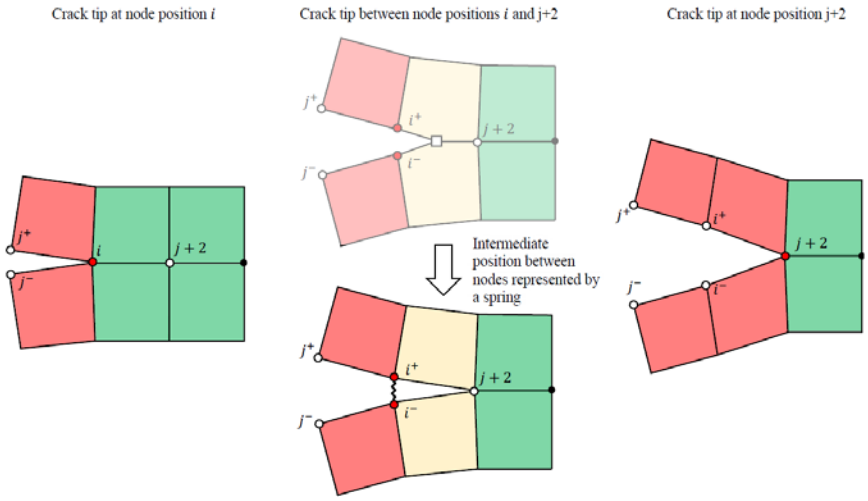

Fig. 2 Progressive release procedure and the use of a spring-like kinematic constraint to represent intermediate crack positions.

For a linear elastic case, assuming self-similar conditions as the crack propagates, the force $F^i_{z_{max}}$ will linearly decrease:

$$F^i_z = F^i_{z_{max}} \left(1 - \frac{\Delta A}{A^i}\right) = F^i_{z_{max}}(1 - d) \tag{7}$$

where ΔA represents an intermediate crack position and the normalized crack position $d \in [0,1]$ is defined as $d = \frac{\Delta A}{A^i}$, such that if $d = 1$ the node is completely released, and force F^i_z at the node pair i reduces to zero. Using the same assumptions, a relationship similar to Eq. (7) can be written for the displacement jump:

$$\delta^i_z = \delta^j_{z_{max}} d \tag{8}$$

where δ^i_z is the displacement jump at node position i, which will equal $\delta^j_{z_{max}}$ when the node pair is completely released. Alternatively, the relationships given in (7) and (8) can be combined and written as:

$$F^i_z = m_z \delta^i_z + b_z \tag{9}$$

where $m_z = -\frac{F^i_{z_{max}}}{\delta^j_{z_{max}}}$ and $b_z = F^i_{z_{max}}$. For a given value d, Eq. (9) can also be written as:

$$F_z^i = k_z \delta_z^i = m_z \left(1 - \frac{1}{d}\right) \delta_z^i \tag{10}$$

and hence the stiffness of the spring k_z between node pair i^+ and i^- can be expressed as:

$$k_z = m_z \left(1 - \frac{1}{d}\right) \tag{11}$$

Equations (9) and (10) are represented graphically in Fig. 3 for a partially released case, i.e., $d \neq 0$.

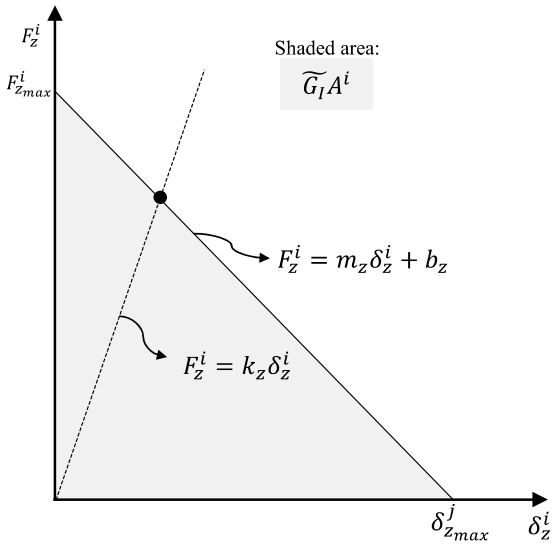

Fig. 3 Progressive release relationship between force and displacement jump, Eqs. (9), (10).

Furthermore, Eq. (10) can be written generally for all degrees of freedom as:

$$\boldsymbol{f}_{VCCT}^i = \boldsymbol{M} \left(1 - \frac{1}{d}\right) \boldsymbol{\delta}^i \tag{12}$$

where:

$$\boldsymbol{M} = \begin{bmatrix} m_x & 0 & 0 \\ 0 & m_y & 0 \\ 0 & 0 & m_z \end{bmatrix} \tag{13}$$

Typically, delaminations grow under generic mixed-mode conditions. Assuming that the crack starts to grow past nodal position i with $\widetilde{G_I}$ and $\widetilde{G_{II}}$ calculated using VCCT:

$$\widetilde{G_I} = \frac{1}{2A^i} F^i_{z_{max}} \, \delta^j_{z_{max}}$$

$$\widetilde{G_{II}} = \frac{1}{2A^i} F^i_{x_{max}} \delta^j_{x_{max}} \tag{14}$$

Mode III is ignored for simplicity, but can be considered in a similar fashion. To represent self-similar growth under mixed-mode conditions, the relationship between force and displacement as the crack grows past a given node pair, (Eqs. (9) and (10)) can be written separately for z and x directions, as illustrated in Fig. 4. Note that these relationships are different for z and x directions. Assume that conditions change during the progressive release, and the new $\widetilde{G_I}^{new}$, $\widetilde{G_{II}}^{new}$ are different from the initial $\widetilde{G_I}$, $\widetilde{G_{II}}$ that led to a finite amount of growth. This can occur as the crack propagates in a non-self-similar fashion. Alternatively, it can also occur as a result of unloading after some initial release, and re-loading with different loading conditions. Despite the different loading conditions, if no growth occurs during unloading and re-loading according to the fracture criterion/growth law assumed, the spring stiffnesses, k_z^U and k_z^R should be identical and equal to k_z:

$$k_z^U = m_z^U \left(1 - \frac{1}{d^R}\right)$$

$$k_z^R = m_z^R \left(1 - \frac{1}{d^U}\right) \tag{15}$$

where the superscripts (U) and (R) designate variables associated with unloading (U) and re-loading (R).

$$k_z^U = k_z^R = k_z \tag{16}$$

In addition, since no growth occurs,

$$d^U = d^R = d \tag{17}$$

Recalling Eqs. (11), (16) and (17) are satisfied if:

$$m_z^U = m_z^R = m_z \tag{18}$$

and thus m_z is considered constant during the progressive release. Using similar arguments, m_x and m_y are also considered constant during the progressive release. This guarantees that no crack growth/healing occurs as a result of variation of loading conditions alone, without a fracture criterion or growth law being met. Using this condition, and Eqs. (7), (8), (10) and (14), G_I^p, G_{II}^p, and G_{III}^p are determinable for a partially released node (the superscript p indicates partial release conditions):

$$G_I^p = -\frac{m_z(\delta_z^i)^2}{2d^2A^i}$$

$$G_{II}^p = -\frac{m_x(\delta_x^i)^2}{2d^2A^i} \tag{19}$$

$$G_{III}^p = -\frac{m_y(\delta_y^i)^2}{2d^2A^i}$$

As a result, if the loading conditions change, the unloading curves described by Eq. (19) may shift, since $\widetilde{G_I} = G_I^p$ and $\widetilde{G_{II}} = G_{II}^p$ may vary, but the slopes remain constant as illustrated in Fig. 4.

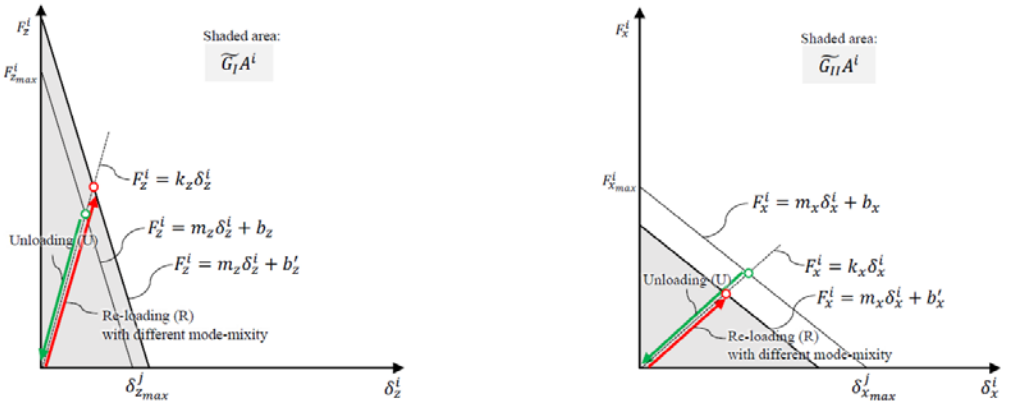

Fig. 4 Variation of the progressive release relationships as a consequence of a change in mode mixity due to unloading and re-loading with different loading conditions.

In the implementation discussed above, an initial infinite penalty stiffness, k_p, (here the subscript p indicates "penalty") was assumed between node pairs that have not yet released. Figure 5 illustrates an implementation with a finite initial penalty stiffness. In this case, the force F_z^i at the node pair i is given by:

$$F_z^i = \begin{cases} k_p\delta_z^i, & \delta_z^i \le \delta_{z_0}^i \\ m_z\left(\dfrac{d-1}{d-\dfrac{m_z}{k_p}}\right)\delta_z^i, & \delta_z^i \ge \delta_{z_0}^i \end{cases} \tag{20}$$

where $\delta_{z_0}^i = \frac{F_{z_{max}}^i}{k_p}$, and:

$$m_z = -\frac{F_{z_{max}}^i}{\delta_{z_{max}}^j - \delta_{z_0}^i} = \frac{F_{z_{max}}^i}{\dfrac{F_{z_{max}}^i}{k_p} - \delta_{z_{max}}^j} \tag{21}$$

and:

$$d = \frac{\delta_z^i - \delta_{z_0}^i}{\delta_{z_{max}}^j - \delta_{z_0}^i}, for\ \delta_z^i \geq \delta_{z_0}^i \tag{22}$$

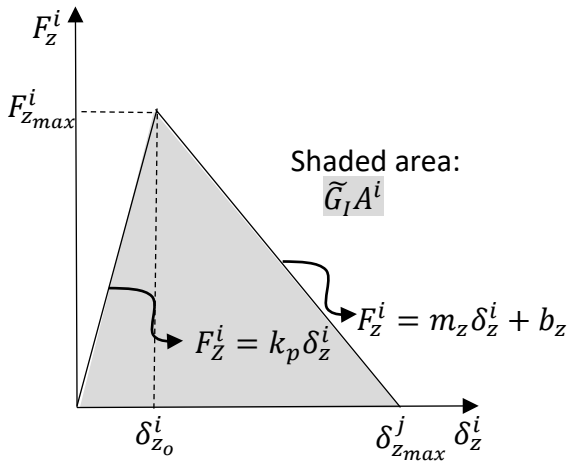

Fig. 5 Progressive release relationship between force and displacement jump with finite initial penalty stiffness.

Finally, the energy release rate for nodes that have started their partial release, and hence $\delta_z^i \geq \delta_{z_o}^i$, can be determined by:

$$G_I^p = -\frac{m_z(\delta_z^i)^2}{2A^i}\left[\frac{1 - \frac{m_z}{k_p}}{\left(d - \frac{m_z}{k_p}\right)^2}\right] \tag{23}$$

Comparing Eqs. (20) and (23) to Eqs. (10) and (19), one can conclude that the finite initial penalty stiffness does not affect the previous arguments, but leads to modified expressions for progressive release (Eq. (20)) and energy release rate (Eq. (23)). Equations (20) and (23) can be generalized and written for all directions, obtaining equivalent relationships to Eqs. (12) and (19), which are omitted for brevity in this paper.

Jacobian Development

Consider the equilibrium of a generic linear elastic solid subject to external forces, $\mathbf{f}_{\text{ext}}$, with internal stresses, $\boldsymbol{\sigma}$, in which partially released springs, $\mathbf{f}_{\text{VCCT}}(\boldsymbol{\delta})$, are included to represent intermediate crack positions:

$$\int_{\Omega} \boldsymbol{\sigma}\, d\Omega + \mathbf{f}_{VCCT}(\boldsymbol{\delta}) + \mathbf{f}_{ext} = 0 \tag{24}$$

In order to solve a nonlinear system of equations using a numerical method, the derivative of the left-hand-side is often required to help determine the solution. This derivative is commonly referred to as the Jacobian. For a linear-elastic analysis and a corresponding finite element method discretization, all terms in Eq. (24) are a linear function of the displacements except $\mathbf{f}_{VCCT}$. See [10] for further detail. The derivative of $\mathbf{f}_{VCCT}$ with respect to the displacement jumps $\boldsymbol{\delta}$ can be written as:

$$\boldsymbol{J} = \frac{\partial \boldsymbol{f}_{VCCT}}{\partial \delta} = \begin{bmatrix} \frac{\partial f_{VCCT-x}}{\partial \delta_x} & \frac{\partial f_{VCCT-x}}{\partial \delta_y} & \frac{\partial f_{VCCT-x}}{\partial \delta_z} \\ \frac{\partial f_{VCCT-y}}{\partial \delta_x} & \frac{\partial f_{VCCT-y}}{\partial \delta_y} & \frac{\partial f_{VCCT-y}}{\partial \delta_z} \\ \frac{\partial f_{VCCT-z}}{\partial \delta_x} & \frac{\partial f_{VCCT-z}}{\partial \delta_y} & \frac{\partial f_{VCCT-z}}{\partial \delta_z} \end{bmatrix} \tag{25}$$

In the remainder of the paper the term Jacobian refers to its terms as given by Eq. (25). For infinite initial penalty stiffness, k_p, and using Eq. (12), where the superscript i is omitted for convenience:

$$\begin{aligned}
\frac{\partial f_{VCCT-x}}{\partial \delta_x} &= m_x\left(1-\frac{1}{d}\right) - m_x\delta_x\frac{\partial}{\partial \delta_x}\left(\frac{1}{d}\right) \\
\frac{\partial f_{VCCT-x}}{\partial \delta_y} &= -m_x\delta_x\frac{\partial}{\partial \delta_y}\left(\frac{1}{d}\right) \\
\frac{\partial f_{VCCT-x}}{\partial \delta_z} &= -m_x\delta_x\frac{\partial}{\partial \delta_z}\left(\frac{1}{d}\right) \\
\frac{\partial f_{VCCT-y}}{\partial \delta_x} &= -m_y\delta_y\frac{\partial}{\partial \delta_x}\left(\frac{1}{d}\right) \\
\frac{\partial f_{VCCT-y}}{\partial \delta_y} &= m_y\left(1-\frac{1}{d}\right) - m_y\delta_y\frac{\partial}{\partial \delta_y}\left(\frac{1}{d}\right) \\
\frac{\partial f_{VCCT-y}}{\partial \delta_z} &= -m_y\delta_y\frac{\partial}{\partial \delta_z}\left(\frac{1}{d}\right) \\
\frac{\partial f_{VCCT-z}}{\partial \delta_x} &= -m_z\delta_z\frac{\partial}{\partial \delta_x}\left(\frac{1}{d}\right) \\
\frac{\partial f_{VCCT-z}}{\partial \delta_y} &= -m_z\delta_z\frac{\partial}{\partial \delta_y}\left(\frac{1}{d}\right) \\
\frac{\partial f_{VCCT-z}}{\partial \delta_z} &= m_z\left(1-\frac{1}{d}\right) - m_z\delta_z\frac{\partial}{\partial \delta_z}\left(\frac{1}{d}\right)
\end{aligned} \tag{26}$$

If the damage parameter d is constant, the off-axis terms vanish, resulting in a symmetric Jacobian with only diagonal terms. If the damage parameter d increases, the Jacobian depends on the mixed mode law used.

For the linear power mixed mode law, during crack extension:

$$\frac{G_I}{G_{IC}} + \frac{G_{II}}{G_{IIC}} + \frac{G_{III}}{G_{IIIC}} = 1 \tag{27}$$

By substituting Eq. (19) into Eq. (27) and rearranging, the damage parameter can be expressed as

$$d^2 = \frac{-m_z {\delta_z}^2}{2AG_{IC}} + \frac{-m_x {\delta_x}^2}{2AG_{IIC}} + \frac{-m_y {\delta_y}^2}{2AG_{IIIC}} \tag{28}$$

resulting in

$$\begin{aligned}
\frac{\partial f_{VCCT-x}}{\partial \delta_x} &= m_x\left(1-\frac{1}{d}\right) - \frac{{m_x}^2 {\delta_x}^2}{2d^3 AG_{IIC}} \\
\frac{\partial f_{VCCT-x}}{\partial \delta_y} &= -\frac{m_x m_y \delta_x \delta_y}{2d^3 AG_{IIIC}} \\
\frac{\partial f_{VCCT-x}}{\partial \delta_z} &= -\frac{m_x m_z \delta_x \delta_z}{2d^3 AG_{IC}} \\
\frac{\partial f_{VCCT-y}}{\partial \delta_x} &= -\frac{m_x m_y \delta_x \delta_y}{2d^3 AG_{IIC}} \\
\frac{\partial f_{VCCT-y}}{\partial \delta_y} &= m_y\left(1-\frac{1}{d}\right) - \frac{{m_y}^2 {\delta_y}^2}{2d^3 AG_{IIIC}} \\
\frac{\partial f_{VCCT-y}}{\partial \delta_z} &= -\frac{m_y m_z \delta_y \delta_z}{2d^3 AG_{IC}} \\
\frac{\partial f_{VCCT-z}}{\partial \delta_x} &= -\frac{m_x m_z \delta_x \delta_z}{2d^3 AG_{IIC}} \\
\frac{\partial f_{VCCT-z}}{\partial \delta_y} &= -\frac{m_y m_z \delta_y \delta_z}{2d^3 AG_{IIIC}} \\
\frac{\partial f_{VCCT-z}}{\partial \delta_z} &= m_z\left(1-\frac{1}{d}\right) - \frac{{m_z}^2 {\delta_z}^2}{2d^3 AG_{IC}}
\end{aligned} \tag{29}$$

Note that the Jacobian for d increasing is not generally symmetric because the critical energy release rates for each mode (G_{IC}, G_{IIC}, G_{IIIC}) are not normally equal.

For the B-K (Benzeggagh-Kenane) mixed mode law [11], during crack extension:

$$G_T = G_{IC} + \left[G_{IIIC}\frac{G_{III}}{G_T} + G_{IIC}\frac{G_{II}}{G_T} - G_{IC}\left(\frac{G_{II}+G_{III}}{G_T}\right)\right]\left(\frac{G_{II}+G_{III}}{G_T}\right)^{n-1} \tag{30}$$

By substituting Eq. (19) into Eq. (30) and rearranging, the damage parameter can be expressed as

$$\begin{aligned}
d = {} & \left(-m_z {\delta_z}^2 - m_x {\delta_x}^2 - m_y {\delta_y}^2\right)^{\frac{n+1}{2}} \\
& / \Big\{2A\Big[G_{IC}\left(-m_z {\delta_z}^2 - m_x {\delta_x}^2 - m_y {\delta_y}^2\right)^n \left(-G_{IIIC} m_z {\delta_z}^2\right. \\
& \left. - G_{IIC} m_x {\delta_x}^2\right)\left(-m_x {\delta_x}^2 - m_z {\delta_z}^2\right)^{n-1} - G_{IC}\left(-m_x {\delta_x}^2 - m_z {\delta_z}^2\right)^n\Big]\Big\}^{\frac{1}{2}}
\end{aligned} \tag{31}$$

The Jacobian terms can be found by substituting the above equation for *d* into Eq. (29). For a finite initial penalty stiffness, k_p, similar equations can be developed. Unfortunately, the developed equations may need to be solved numerically.

RESULTS

This section presents two sets of results. The first consists of an assessment and demonstration of the need to combine VCCT with progressive release to be able to

obtain a generic mesh-independent crack propagation capability when using VCCT without re-meshing. The second set of results explores further the novel formulation proposed in the present paper and its effect on the convergence of the non-linear solver used. All results were obtained using ABAQUS/Standard (Implicit).

Progressive Release and Mesh-Independent Crack Propagation

Two DCB models with identical dimensions but different meshes are shown in Figure 6. Each uses the material properties listed in Tables I and II. The model shown in Figure 6a has an overall structured mesh with mesh lines approximately aligned with the predominantly straight crack front that develops in DCB specimens. In Figure 6b however, the mesh is skewed or angled with $\theta = 22.5°$, such that it does not necessarily conform to a predominantly straight crack front.

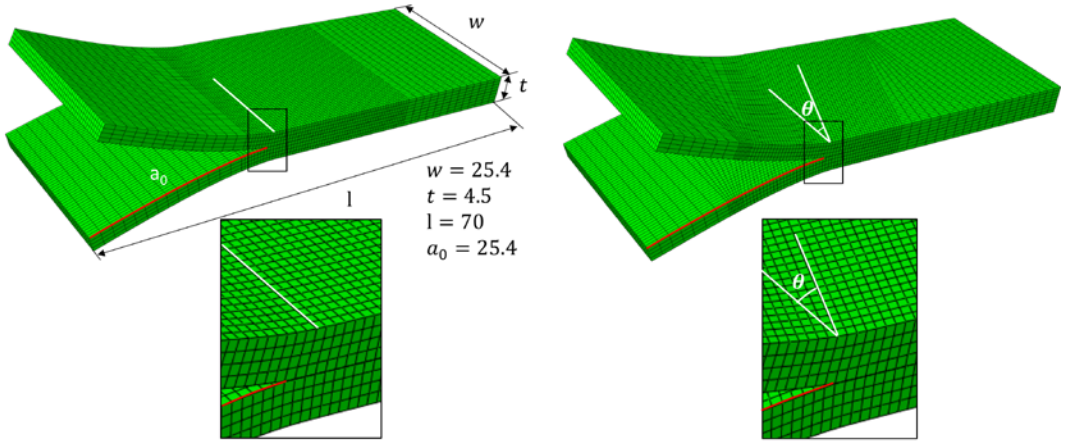

(a) DCB straight mesh (b) DCB angled mesh
(All dimensions in mm and given in the undeformed configuration)

Figure 6. DCB models used. Element size in refined region: $el_{size} = 0.5$ mm.

TABLE I. ELASTIC PROPERTIES [12]

E_{11} [GPa]	$E_{22} = E_{33}$ [GPa]	$G_{12} = G_{13}$ [GPa]	G_{23} [GPa]	$\nu_{12} = \nu_{13}$ [−]	ν_{23} [−]
161	10.38	5.17	3.98	0.32	0.44

TABLE II. FRACTURE TOUGHNESS PROPERTIES [12]

G_{Ic} [N.mm^{-1}]	G_{IIc} [N.mm^{-1}]
0.212	0.774

Figure 7 summarizes the results obtained with the models outlined in Fig. 6. For each of the models in Fig. 6, two simulations were performed, with and without using progressive release. For the straight mesh case, the simulation performed without using progressive release, labeled “Straight Mesh”, agrees well with the benchmark obtained from [12]. However, there are large steps associated with a significant number of nodes being instantly released simultaneously when $G_T > G_c$. For the angled mesh case, however, the simulation performed without using progressive release leads to a

significant under-prediction of the benchmark. Refining the mesh does not lead to an attenuation of the difference. If progressive release is used, the two simulations performed using angled and straight meshes give approximately identical results that agree closely with the benchmark results. The only difference is that in the simulation using an angled mesh, labeled "Progressive Release – Angled", the load-displacement starts tapering earlier near the peak load. This is caused by the initial crack shape not being straight. In this model, the initial crack shape is assumed to conform to the element boundaries. Since the element boundaries are not straight this results in an initial crack front with a zig-zag shape.

These results suggest that a mesh-independent solution cannot be obtained with instant release, and that a progressive release scheme provides an avenue to ensure mesh independence without requiring re-meshing.

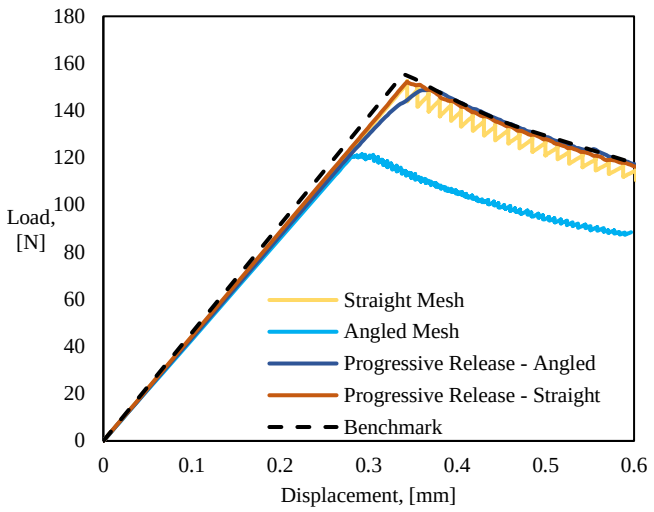

Fig. 7 DCB results comparing progressive release and instant release algorithms for angled and straight meshes.

Convergence Assessment: Mode I and Mixed Mode I/II

In present section, the convergence behavior as a function of three different approximations for the Jacobian (unsymmetric, symmetric and diagonal) is compared. The unsymmetric formulation uses the Jacobian **J** as defined in Eq. (29), and requires the activation in Abaqus of the option to solve equations using an unsymmetric solver. In the symmetric option, the Jacobian is assumed to be given by $\boldsymbol{J_{ij}^{Sym}} = \frac{J_{ij}+J_{ji}}{2}$**.** Finally, in the diagonal formulation, all terms of the Jacobian $\boldsymbol{J^{Diag}}$ are assumed to be zero except for the diagonal terms, which are set equal to the diagonal terms of **J**. Two assessments were performed using DCB and MMB models with dimensions and boundary conditions as shown in Figure 8. The models are 3D with a single element across the width. The results obtained are shown in Figures 9 and 10, where they are compared against benchmarks obtained from [12].

As shown in Fig. 9, for Mode I, all approximations for the Jacobian seem to lead to accurate results. The CPU times did not vary significantly for the models used, however it seems the unsymmetric option led to slightly longer CPU times. However, for the

mixed mode case with $\frac{G_{II}}{G_T} = 0.5$, the solutions using the diagonal and symmetric Jacobian did not converge. This occurred because the Jacobian is unsymmetric in the presence of mixed-mode conditions. For both cases, identical models simulated with the native Abaqus VCCT did not converge without the use of contact damping, following [12], or global stabilization.

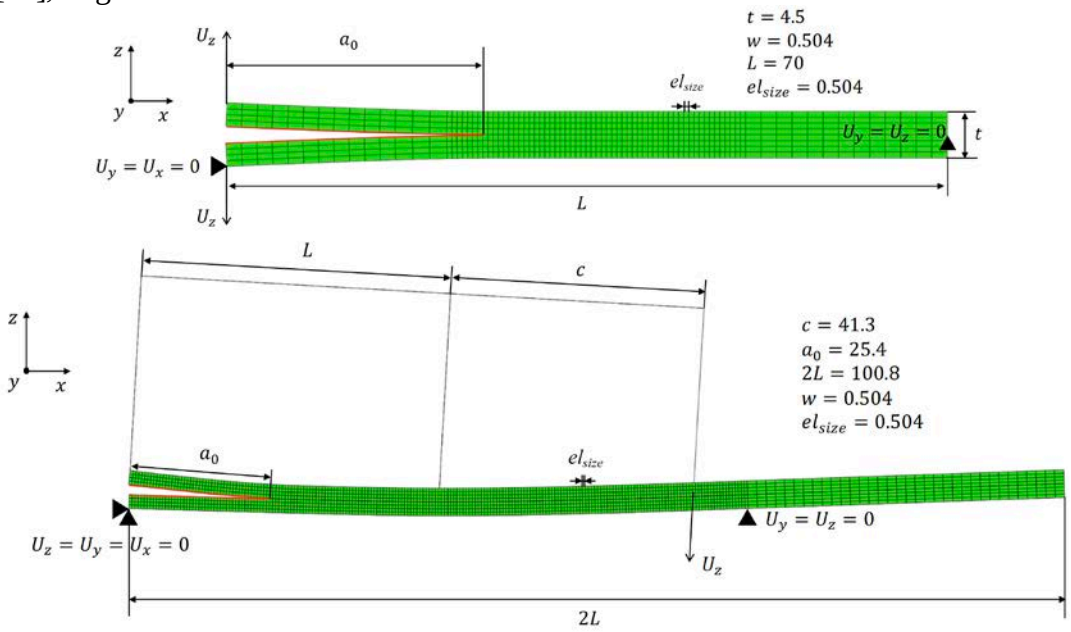

(All dimensions in mm and given in the undeformed configuration)

Figure 8 DCB and MMB models. 3D models, with one element along the width.

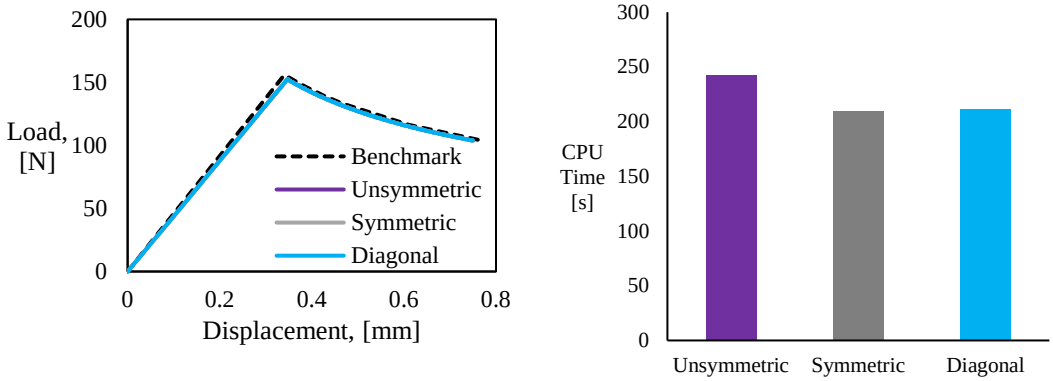

Figure 9 DCB results obtained using different Jacobian approximations.

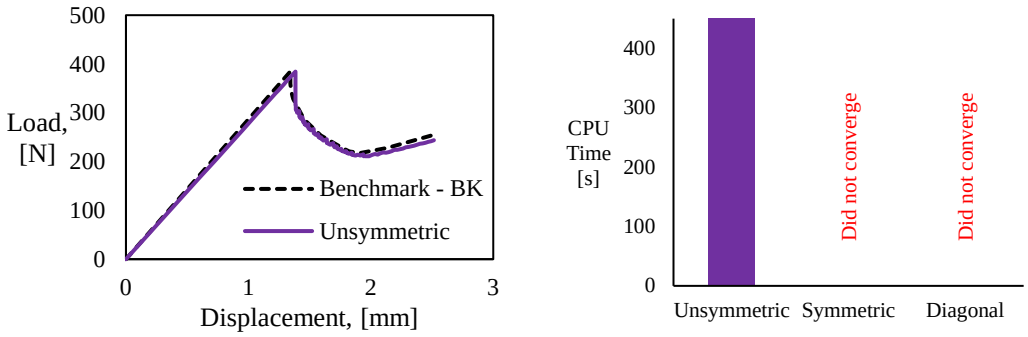

Figure 10 MMB, $\frac{G_{II}}{G_T} = 0.5$ results obtained using different Jacobian approximations.

SUMMARY

The present study shows that performing a gradual nodal release is key to model delamination propagation with VCCT without re-meshing. This procedure, under quasi-static loading conditions, requires solving a nonlinear-system of equations. To help solve the non-linear system of equations, a detailed derivation of the Jacobian terms associated with the progressive nodal release was performed. Results obtained indicate that convergence of the algorithm is directly linked to the accuracy of the Jacobian approximation used. Other strategies, such as damping and overall stabilization, can be used to address convergence issues. The present study suggests that their use may, in some cases, be circumvented by improving the Jacobian formulation used, and through a formal understanding of its dependence on the assumed material model. Overall these findings have the potential to improve robustness of the non-linear solution procedure used, decreasing the trial and error process needed to arrive at a solution and the overall uncertainty regarding the accuracy of a given solution for cases where no benchmark or analytical solution is available.

ACKNOWLEDGEMENTS

This report is based upon work supported by NASA under Award No. NNL09AA00A. Any opinions, findings, and conclusions or recommendations expressed in this report are those of the author(s) and do not necessarily reflect the views of the National Aeronautics and Space Administration.

REFERENCES

1. E.F. Rybicki, M.F. Kanninen. “A finite element calculation of stress intensity factors by a modified crack closure integral,” *Engineering Fracture Mechanics*, 9(4):931–938, 1977.
2. I.S. Raju, R. Sistla, and T. Krishnamurthy. “Fracture mechanics analyses for skin-stiffener debonding,” *Eng. Fract. Mech.* 54(3):371–385, 1996.
3. E.H. Glaessgen, I.S. Raju, and C.C. Poe. “Fracture mechanics analysis of stitched stiffener-skin debonding,” The *39th AIAA/ASME/ASCE/AHS/ASC Structures, Structural Dynamics and Materials Conference*, Long Beach, California, AIAA 98-2022, April 20–23, 1998.
4. R. Krueger. “Virtual crack closure technique: history, approach, and applications,” *Applied Mechanics Reviews*, 57(2):109 – 143, 2004.
5. M.F.S.F. De Moura, J.P.M. Gonçalves, A.T. Marques, and P.M.S. Tavares De Castro. “Modeling compression failure after low velocity impact on laminated composites using interface elements,” *Journal of Composite Materials*, 31(15):1462 – 1479, 1997.
6. P.P. Camanho and C.G. Dávila. “Mixed-mode decohesion finite elements for the simulation of delamination in composite materials,” Technical report, NASA-TM-2002-211737, National Aeronautics and Space Administration, 2002.
7. G.E. Mabson, L.R. Deobald, B. Dopker, D.M. Hoyt, J.S. Baylor, D.L. Graesser. “Fracture interface elements for static and fatigue analysis,” In *16th International conference on composite materials*, Kyoto, July 2007.

8. L. Deobald, G. Mabson, B. Dopker, and D. Graesser. “Interlaminar fatigue elements for crack growth based on virtual crack closure technique,” In *Proceedings of the 48th AIAA/ASME/ASCE/AHS/ASC Structures, Structural Dynamics and Materials Conference*, 2007.
9. *Abaqus Analysis User’s Manual*, Abaqus/Standard DSS Simulia, 6.17 edition, 2017.
10. N.V. De Carvalho, R. Krueger, G.E. Mabson, and L.R. Deobald. “Combining Progressive Nodal Release with the Virtual Crack Closure Technique to Model Fatigue Delamination Growth Without Re-meshing,” *AIAA-2018-1468, SCITECH 2018*, Kissimmee Fl, Jan 8-12, 2018.
11. M. L. Benzeggagh and M. Kenane, “Measurement of mixed-mode delamination fracture toughness of unidirectional glass/epoxy composites with mixed-mode bending apparatus,” *Composites Science and Technology*, vol. 56, pp. 439-449, 1996.
12. R. Krueger, “A summary of benchmark examples and their application to assess the performance of quasi-static delamination propagation prediction capabilities in finite element codes,” *Journal of Composite Materials*, vol. 49, pp. 3297-3316, 2015.